Construction of Cellulose/Carboxymethyl Chitosan Hydrogels for Potential Wound Dressing Application

Yi Guo
Wuhan Textile University - Yangguang Campus: Wuhan Textile University
Chuanyin Zhao
Wuhan Textile University
Chao Yan (yanchao18306@163.com)
Wuhan Textile University
Li Cui
Wuhan Textile University

Research Article

Keywords: Cellulose, Carboxymethyl chitosan, LiOH/urea aqueous solutions, Hydrogels, Wound dressing

Posted Date: April 30th, 2021

DOI: https://doi.org/10.21203/rs.3.rs-424847/v1

Abstract

In this study, novel cellulose/carboxymethyl chitosan (CMCS) composite hydrogels were constructed by blending cellulose and CMCS in LiOH/urea aqueous solutions, and then cross-linking with epichlorohydrin. The structure and morphology of the composite hydrogels were characterized by Fourier transform infrared spectroscopy (FT-IR), wide-angle X-ray diffraction (WXRD), thermo-gravimetric analysis (TGA), and scanning electron microscopy (SEM). The results revealed that the chemical cross-linking reaction between cellulose and CMCS occurred in the hydrogel, and CMCS contributed to the enhancement of pore size, whereas cellulose as a strong backbone in the hydrogel to support the pore wall. The mechanical strength of the composite hydrogels increased with the cellulose content, while the equilibrium swelling ratio and antibacterial activity increased with the CMCS content. The composite hydrogels had no cytotoxicity towards L929 cells, suggesting good biocompatibility. All these results indicate that cellulose/CMCS composite hydrogels can be effectively used as a material in wound dressing.

1. Introduction

Recently, great efforts are being invested to develop new materials for healing the damaged skin rapidly and relieving suffering (Rowan et al. 2015). Wound dressings had been developed from a simple plain textile strip to engineered composite materials such as gauzes, membranes, sponges, gels, hydrocolloids and hydrogels (Pinho and Soares 2018). As an ideal dressing material, it should be readily operated and painlessly removed, absorbing fluids and exudes effectively, haemostaticity, maintaining a moist wound environment, showing higher gas permeation and preventing microbial infection (Cheng et al. 2019; Chen et al. 2018; Capanema et al. 2018). Non-toxicity, favorable biocompatibility, high elasticity and also adequate mechanical strength are the other desired properties of an ideal wound dressing (Naseri et al. 2015).

Properties such as biodegradability, biocompatibility, similarity to macromolecules recognized by the human body and promoting cell growth make some natural polymers suitable for widely using in biomedical applications (Gonzalez et al. 2014). In the last decade, natural polymers, like polysaccharides and derivatives (chitin, chitosan, alginates, heparin and cellulose), proteoglycans and proteins (collagen, gelatin, fibrin, keratin), have been developed as wound dressings (Mogoşanu and Grumezescu 2014; Ganesan 2017; Ye et al. 2018; Jayakumar et al. 2011; Clark 2018; Ge et al. 2018; Li et al. 2016; Deepachitra et al. 2014; Singaravelu et al. 2015).

Chitosan, a positively charged polysaccharide obtained by partial N-deacetylation of chitin, is known to possess unique properties including antibacterial activity, wound healing, hemostasis, and is widely used in Celox and Hemcon (Chen et al. 2018; Pourshahrestani et al. 2017). However, the fact that chitosan shows poor solubility in neutral water limits its applications in biomedicine, and the chemical modification of chitosan requires toxic organic substances. Carboxymethyl chitosan (CMCS), one of the chitosan derivatives with high solubility under physiological conditions, inherited the basic merits from

chitosan that make it to be a potential candidate for wound dressings. Wang et al. reported that CMCS coated carboxymethylated cotton showed better hemostatic capacity than the cotton fabric (Wang et al. 2020). However, the water-soluble polymers are too weak to be used by itself for wound dressing or scaffolding application, many attempts have been made to increase the structural strength of CMCS. CMCS films were crosslinked by microwave technique to prolong their dimensional integrity for possible use in wound care applications (Zhang et al. 2019). CMCS-based hydrogel reinforced with modified cellulose nanocrystal for deep partial thickness burn wound healing was developed by Huang et al. (2018). The hydrogels exhibit high self-healing efficiency, injectability, good mechanical strength, and a high equilibrium swelling ratio of 350% while maintaining integrity. Furthermore, natural polymers such as gelatin have been combined with CMCS by radiation crosslinking, which was efficient to stabilize the hydrogel structure and prolong the degradation time. The CMCS/gelatin hydrogel could induce granulation tissue formation and accelerate the wound healing (Huang et al. 2013).

Because their biocompatible and biodegradable, cellulose and its derivatives have been also developed for wound dressing materials (Harkins et al. 2014; Cheng et al. 2018; Capanema et al. 2018; Fawal et al. 2018). Moreover, cellulose with stiffness molecular chain could be used effectively to strengthen the materials (Harkins et al. 2014; He et al. 2018). Thus, we attempted to introduce cellulose as a backbone into CMCS matrix, and fabricate novel cellulose/CMCS composite hydrogels for use as wound dressing material. In the present work, cellulose and CMCS were dissolved in LiOH/urea aqueous solution to construct macroporous hydrogels by using epichlorohydrin as cross-linker. The structure and morphology of cellulose/CMCS composite hydrogels were characterized by Fourier transform infrared (FT-IR) spectroscope, wide-angle X-ray diffraction (WXRD), thermogravimetric analysis (TGA) and scanning electron microscope (SEM). The swelling behavior and the mechanical properties of the composite hydrogels were investigated and discussed. In addition, the hydrogels were evaluated for use as wound dressing material.

2. Experimental Section

2.1 Materials

Cotton linter pulp was supplied by Hubei Chemical Fiber Co. Ltd. (Xiangfan, China). The weight-average molecular weight (M_W) was determined by static laser light scattering (DAWN DSP, Wyatt Technology Co., US) in NaOH/urea aqueous solution to be $6.3 \cdot 10^4$. Chitosan (CS, $5 \cdot 10^4$, degree of deacetylation is 93%) was purchased from Qingdao Yunzhou Biochemistry Co., Ltd. (Qingdao, China). NaOH, isopropanol, ethanol, monochloroacetic acid, $LiOH{\bullet}H_2O$, urea, epichlorohydrin (ECH) and all other reagents (Shanghai Chemical Reagent Co. Ltd., China) were analytical grade and used without further purification.

2.2 Preparation of CMCS

CMCS was prepared according to Wahid et al. (2017) with slight changes. Initially, to make CS swollen and alkalized, 1 g of purified chitosan was dispersed in isopropanol (20 mL) and 40 wt% NaOH aqueous

solution was added at room temperature. After alkalization for 2 h, 1.5 g monochloroacetic acid dissolved in 2 ml isopropanol was added dropwise for 30 min under continuous stirring and the reaction mixture was stirred for 2 h at 60 ℃. The reaction was stopped by adding an excess of 70% ethanol, then the reaction mixture was neutralized with 10% acetic acid. The product was filtered and washed several times with 70–90% ethanol. Finally, the obtained powder was dried and stored for further use. The degree of substitution of CMCS was about 0.70, which was determined by using the potentiometric titration method (Huang et al. 2015).

2.3 Preparation of the cellulose/CMCS composite hydrogels

The cellulose solution was prepared according to the previous report He et al. (2018) as follows. 5 g cotton linter pulp was completely dissolved in the precooled 95 g of 8 wt% LiOH•H_2O/15 wt% urea aqueous solutions at -12.8 ℃ to obtain 5 wt% cellulose solutions. CMCS was dissolved in the same solvent at room temperature to obtain 5 wt% CMCS solutions. The cellulose and CMCS solutions were mixed, and 1ml ECH as the crosslinking agent was added dropwise into 10 g solution in an ice bath under mechanical stirring for 30 min to obtain a homogeneous solution. The mixed solutions were kept at 5 ℃ for 12 h to form gels. Finally, gels were washed with distilled water to obtain the hydrogels samples, which were coded as Gel0, Gel1, Gel2, Gel3, Gel4 and Gel5 according to cellulose/CMCS weight ratio of 10/0, 9/1, 8/2, 7/3, 6/4 and 5/5, respectively.

2.4 Characterization

The samples were freeze-dried, cut into powder, and vacuum-dried for 48 h at 60 ℃ before measurement. FT-IR spectra were obtained by the KBr disk technique using a Fourier-transform infrared spectrometer (Perkin Elmer Spectrum One, Wellesley, MA) in the wavelength range from 4000 to 400 cm^{-1}. The wide-angle X-ray diffraction (WAXD) patterns with Cu K_α radiation (λ = 0.15405 nm) at 40 kV and 30 mA were recorded on an XRD instrument (D8, Bruker AXS GmbH, Karlsruhe, Germany) in the region of 2θ from 6° to 40° with scanning rate of 2°/min. Thermogravimetric analysis (TGA) was carried out on a NETZSCH STA 449C thermal analyzer (NETZSCH, Germany) at heating rate of 10 ℃/min from room temperature to 500 ℃ under nitrogen atmospheres. Scanning electron microscope (SEM) was taken with on a JSM-6510 scanning electron microscope (JEOL, Japan) at an accelerating voltage of 15 kV. The hydrogels swollen to equilibrium in distilled water at 37 ℃ for 24 h were frozen in liquid nitrogen, snapped immediately, and then freeze-dried using a lyophilizer. The cross-section of the hydrogels was sputtered with gold, observed, and photographed.

The compression strength of hydrogels in the equilibrium swelling state was measured on a universal tensile machine (CMT 6503, Shenzhen SANS, China) according to ISO527-3-1995 (E). The dimension of cylinder samples was about 10mm (D)×10mm (H), the crosshead speed was 2 mm/min. The results are averages of five measurements.

The gravimetric method was employed to measure the swelling ratios of the hydrogels in distilled water at 37 ℃. The equilibrium swelling ratio (ESR) was calculated as

$$ESR = W_s / W_d \quad (1)$$

where W_s and W_d represent the weight of swollen hydrogel at swelling equilibrium and freeze-dried gel, respectively. All experiments were performed at least three times.

Water uptake (WU) is applied to clarify the reswelling. To measure WU, the freeze-dried gels were immersed in distilled water at 37 ℃. At regular time intervals, the samples were taken out and weighted after wiping excess water on the surface. The WU value was calculated as

$$WU\ (\%) = (W_t - W_d)/W_s \cdot 100\% \quad (2)$$

where W_t is the weight of the re-swollen gel at time t, W_d and W_s are same as Eq. (1).

2.5 Antibacterial activity test

The antibacterial performance test of the hydrogels was performed similar to the previous report Gonzalez et al. (2014) to evaluate the resistance of the hydrogel against bacteria. Briefly, the dried Gel0, Gel2, Gel3 and Gel5 with the diameter of 1 cm and the height of 1cm were sterilized for 30 min by UV in a clean bench. The sterilized samples were put on the MHA (Mueller-Hinton Agar) that be already solidified. 15 μL of a suspension of bacteria (*Staphylococcus aureus* CMCC 26003 and *Echerichia coli* CMCC 44102) with a concentration of $3.0 \cdot 10^8$ UFC/mL was dropped on the upper surface of hydrogels to culture at 37°C for 24 h in an incubator. The cultured hydrogels were frozen in liquid nitrogen and snapped immediately, and then freeze-dried. The cross-section of the hydrogels was sputtered with gold, and then observed and photographed.

2.6 L929 cell viability assay

The cytotoxicity for hydrogels was evaluated through MTT assay. The freeze-dried hydrogels were cut into powder, sterilized by autoclaving, and then suspended in PBS at 1 mg/mL to culture, with each hole 5000 cells in 200 μL DMEM. After incubating for 48 h, 10 μL MTT was added in each hole for a further 4 h incubation before 200 μL DMSO was added to dissolve the formazan and detected absorption intensity at 570 nm. Cell viability was calculated using the following equation:

$$\text{Cell viability}\ (\%) = (A_{test} \div A_{control}) \times 100\%$$

where A_{test} and $A_{control}$ correspond to the absorbance values of the test and control groups, respectively. In live/dead staining assay, 1 mg/mL hydrogel powder was added into the plate hole to culture at 48 h. After finished, 15 μL (2.5 μM) calcein-AM and 9 μL (2.5 μM) PI were added into the hole to incubate 15 min more at 37℃ 5% CO_2 atmosphere, and observed under Fluorescent Inverted microscope.

3. Results And Discussion

3.1 Appearance and structure of the cellulose/CMCS composite hydrogels

Proposed mechanism for the cross-linking reaction of cellulose and CMCS with ECH in alkali aqueous solution is shown in Scheme 1. Figure 1 shows the photographs of the hydrogels at different states: the original hydrogels (Fig. 1a), the swollen hydrogels in distilled water (Fig. 1b), the dried hydrogels after vacuum-drying the swollen hydrogels (Fig. 1c) and the dried hydrogels swelling in physical saline water for a week (Fig. 1d). Clearly, all original hydrogels (Fig. 1a) were homogeneous, transparent and relatively small, the swollen hydrogels (Fig. 1b) became bigger with the increase of CMCS content. After vacuum-drying, the obtained dried hydrogels (Fig. 1c) with larger shrinkage became looser with the increasing CMCS content. The dried hydrogels were placed in physical saline water for a week, the reswelling hydrogels (Fig. 1d) exhibited a certain mechanical strength which decreased with the increase of CMCS content from Gel0 to Gel5.

The FTIR spectra of the samples of chitosan, CMCS and the hydrogels were shown in Fig. 2. In the infrared spectrum of chitosan, the very strong broad absorption peak around 3437 cm^{-1} is the O-H stretching and overlaps N-H stretching in the same region. The peaks at 2960 – 2870 cm^{-1} correspond to symmetric and asymmetric C-H vibrations. The peaks at 1645 and 1599 cm^{-1} correspond to amide I and II groups, respectively (Andrea et al. 2016). Compared with the FTIR spectrum of chitosan, CMCS showed the characteristic peaks at 1606 cm^{-1} and 1415 cm^{-1}, which corresponded to the respective asymmetric and symmetric stretching vibrations of $-COO^-$ (Wahid et al. 2017; Andrea et al. 2016). Furthermore, the C-O stretching band at 1030 cm^{-1} corresponding to the primary hydroxyl group of chitosan disappeared, which verified a high carboxymethylation of 6-OH (Zhou et al. 2015). The characteristic peak of second hydroxyl group at 1080 cm^{-1} was not changed. These results confirm the carboxymethylation of chitosan. Compared to the cellulose hydrogel without CMCS (Gel0, see Fig. 2b), intense peaks at 1627 cm^{-1} (N-H stretch) and 1418 cm^{-1} (C-O stretch) in the composite hydrogel indicated the presence of $-NH_2$ groups and -COOH groups, respectively (Kim et al. 2016). It revealed that cellulose and CMCS were successfully crosslinked in the hydrogel.

The X-ray diffraction patterns of cellulose, CMCS and Gel3 were studied. As shown in Fig. 3, cellulose displayed distinct diffraction peaks at $2\theta = 14.8°$, 16.3° and 22.6°, which exhibits the cellulose I crystalline from. The diffraction pattern of pure CMCS shows a broad diffraction peak at $2\theta = 21.4°$, representing its amorphous structure (Yan et al. 2011). However, Gel3 exhibited greater amorphous morphology than cellulose and CMCS, and the typical peaks of cellulose and CMCS disappeared. It indicated the chemical cross-linking between cellulose and CMCS occurred in the hydrogel, leading to the destruction of the initial crystalline structure of cellulose and CMCS.

Thermogravimetric analysis (TGA) is a powerful technique to determine the polymers' state and evaluate the inter-molecular interaction between the two polymers in the materials. Figure 4 shows the TG and DTG curves for cellulose, CMCS, the cellulose/CMCS (weight ratio = 7:3) mixture and Gel3 under N_2

atmosphere. The weight loss below 100°C was the release of moisture from the samples. The peak around 270°C of CMCS was attributed to the thermal decomposition of CMCS, whereas the peak at 350°C of cellulose was caused by the cellulose decomposition. The mixture of cellulose and CMCS exhibited two steps of weight loss, which were assigned to the decomposition of CMCS and cellulose, respectively. However, there was only one weight loss step in the range of 220–380°C in the case of Gel3. This further indicated the chemical cross-linking between two polymers occurred in the hydrogel.

Figure 5 shows the SEM images of the cross-section of the freeze-dried, swollen hydrogels. The cross-sections of the hydrogels displayed three-dimensional porous network structure. The average pore size of cellulose hydrogel regenerated from LiOH/urea aqueous solution (Gel0, see Fig. 5a) was about 20 to 30 μm. With an increase of CMCS content, the average pore size of the composite hydrogels increased and exceeded 100 μm, leading to a more open and loose structure. It indicated that the hydrophilic CMCS with -COOH groups contributed the enhancement of pore size, whereas the relatively stiff cellulose acted as a backbone in the hydrogel to support the pore wall (Chang et al. 2010). Therefore, the composite hydrogels have higher swelling ratio.

3.2 Properties of the cellulose/CMCS composite hydrogels

The mechanical properties of cellulose and cellulose/CMCS composite hydrogels have been investigated. The results for the typical compressive modulus-strain curves of the hydrogels at room temperature are shown in Fig. 6. The compressive modulus of cellulose hydrogel was above 155 KPa, and much higher than cellulose hydrogels that were chemically cross-linked and regenerated from NaOH/urea aqueous solution (Chang et al. 2009). As expected, the mechanical strength of the composite hydrogels increased with an increase of cellulose content in the hydrogels. For example, the compressive modulus values of Gel5, Gel4, Gel3 and Gel1 were 39.2, 44.1, 129.8 and 145.2 KPa, respectively. This further proved that cellulose played a key role in supporting the hydrogels, and could be used to improve the mechanical property of CMCS. Therefore, according to the application, the mechanical properties of the composite hydrogels can be controlled by adjusting the cellulose content.

Figure 7 shows the influence of CMCS composition on the equilibrium swelling ratio of the composite hydrogels in distilled water at 37 °C. The composite hydrogels exhibited higher equilibrium swelling ratio than the cellulose hydrogel, indicating the hydrophilic carboxyl group of CMCS could absorb a lot of water to enhance the water absorbing capacity of the hydrogels. With an increasing ratio of CMCS to cellulose in the hydrogels from 1:9 to 5:5, the equilibrium swelling ratio of the composite hydrogels increased rapidly from 33.8 to 154.2 g/g. The composite hydrogels of higher CMCS content possessed the higher ESR, resulting in the enhancement of the space in the hydrogels. It further confirmed that CMCS acted as expander of the pore sizes, which was consistent with the results of SEM.

The reswelling behaviors of the freeze-dried hydrogels in distilled water at 37 °C are illustrated in Fig. 8. The swelling rates of all hydrogels were quickly during the first hour, then became very slow; all hydrogels finally reached the swelling equilibrium in about 4 h. It was a typical biphasic swelling pattern (Chang et al. 2009). The dried cellulose hydrogel showed only 18% water uptake. With an increasing ratio of CMCS

to cellulose in hydrogels from 1:9 to 5:5, the water uptake of dried composite hydrogels increased from 24–58%. These results indicated that the reswelling capabilities of the composite hydrogels increased with the increasing CMCS content, because the bigger pores could be hold during the freeze-drying process.

The antibacterial activity of the composite hydrogels was evaluated by observing the growth of Gram positive and negative bacteria, *S. aureus* and *E. coli*, in the composite hydrogels. SEM images of the cross-sections of the composite hydrogels with different CMCS content after culturing *S. aureus* for 24h are shown in Fig. 9a-d, and Fig. 9a'-c' are larger magnification SEM images. *S. aureus* bacteria colonies appeared on both the cellulose hydrogel (Fig. 9a, a') and the composite hydrogels (Fig. 9b, b', c, c'). Compared with the control sample, the number of bacteria colonies on the hydrogels decreased with the increase of CMCS content. There was nearly no bacteria colony appeared on GEL5 (Fig. 9d). Thus, the antibacterial activity of the composite hydrogels against *S. aureus* apparently increased with the increase of CMCS content. The same results against *E. coli* could be obtained. Therefore, besides acting as expander of the pore sizes, CMCS with the -NH_2 groups can also play an antibacterial role in the composite hydrogels, which helps wounds avoid infection and accelerates wound healing.

MTT assay has been widely used to investigate the cytotoxicity and biocompatibility of materials, which are important properties for wound dressing materials. Figure 10 shows the results of the cytotoxicity of the composite hydrogels towards L929 cells. The cell viabilities of the hydrogels with different cellulose content have no significant difference (Fig. 10a), which demonstrated the excellent cytocompatibility of the composite hydrogels. Moreover, normal cell morphology and uniform cell distribution were observed by fluorescent inverted microscope (see Fig. 10c-h), which further confirmed good biocompatibility of the composite hydrogels. Therefore, the cellulose/CMCS composite hydrogels presented physicochemical properties, antibacterial activity and biocompatibility are suitable for prospective applications in wound healing.

4. Conclusions

Cellulose/CMCS composite hydrogels were successfully fabricated from LiOH/urea aqueous solution via cross-linking with epichlorohydrin. The composite hydrogels possessed macroporous structures and high equilibrium swelling ratio in water. The pore size, the equilibrium swelling ratio and antibacterial activity increased obviously with the CMCS content. The mechanical properties of the composite hydrogels were improved by cellulose. Moreover, the composite hydrogels had no cytotoxicity to the L929 cells. The combination of cellulose containing semi-stiff chain and CMCS containing -COOH and -NH_2 groups constructed the cellulose/CMCS composite materials with high equilibrium swelling ratio, excellent mechanical strength, good antibacterial activity and biocompatibility, which show potential applications in wound dressing.

Declarations

Acknowledgments:

This work was supported by open fund of State Key Laboratory of Bio-Fibers and Eco-Textiles (Qingdao University, No. KF2020205) as well as Scientific Research Programme of Hubei Provincial Department of Education (No. Q20171608). The authors gratefully thank Laboratory of Natural polymer and Polymer Physics (Wuhan University) for assistance with testing cytotoxicity.

Disclosure of potential conflicts of interest:

Conflict of Interest: The authors declare that they have no conflict of interest.

Research involving human participants and/or animals:

This article does not contain any studies with human participants or animals performed by any of the authors.

Informed Consent:

Informed consent was obtained from all individual participants included in the study.

References

1. Andrea L, Roberta S, Danilo M, Luciano M, Diego Palmiro R (2016) Optimization of carboxymethyl chitosan synthesis using response surface methodology and desirability function. Int J Biol Macromol 85:615-624. https://doi.org/10.1016/j.ijbiomac.2016.01.017
2. Capanema N, Mansur A, Jesus A, Carvalho S, Oliveira L, Mansur H (2018) Superabsorbent crosslinked carboxymethyl cellulose-PEG hydrogels for potential wound dressing applications. Int J Biol Macromol 106:1218-1234. http://dx.doi.org/10.1016/j.ijbiomac.2017.08.124
3. Chang C, Duan B, Cai J, Zhang L (2010) Superabsorbent hydrogels based on cellulose for smart swelling and controllable delivery. Eur Polym J 46(1):92-100. https://doi.org/10.1016/j.eurpolymj.2009.04.033
4. Chang C, Duan B, Zhang L (2009) Fabrication and characterization of novel macroporous cellulose-alginate hydrogels. Polymer 50(23):5467-5473. https://doi.org/10.1016/j.polymer.2009.06.001
5. Chen J, Cheng W, Chen S, Xu W, Lin J, Liu H, Chen Q (2018) Urushiol-functionalized mesoporous silica nanoparticles and their self-assembly into a Janus membrane as a highly efficient hemostatic material. Nanoscale 10(48):22818-22829. https://doi.org/10.1039/C8NR05882B
6. Chen Z, Han L, Liu C, Du Y, Hu X, Du G, Shan C, Yang K, Wang C, Li M, Li F, Tian F (2018) A rapid hemostatic sponge based on large, mesoporous silica nanoparticles and N-alkylated chitosan.

Nanoscale 10(43):20234–20245. https://doi.org/10.1039/ c8nr07865c

7. Cheng F, Wu Y, Li H, Yan T, Wei X, Wu G, He J, Huang Y (2019) Biodegradable N, O-carboxymethyl chitosan/oxidized regenerated cellulose composite gauze as a barrier for preventing postoperative adhesion. Carbohyd Polym 207:180-190. https://doi.org/10.1016/j.carbpol. 2018.10.077
8. Cheng H, Li C, Jiang Y, Wang B, Wang F, Mao Z, Xu H, Wang L, Sui X (2018) Facile preparation of polysaccharide-based sponges and their potential application in wound dressing. J Mater Chem B 6(4): 634-640. https://doi.org/10.1039/C7TB03000B
9. Clark M (2018) Alginates in dressings and wound management. In: Rehm B, Moradali M (eds) Alginates and their biomedical applications. Springer Series in Biomaterials Science and Engineering, vol 11. Springer, Singapore, pp 213-222. https://doi.org/10.1007/978-981-10-6910-9_8
10. Deepachitra R, Ramnath V, Sastry TP (2014) Graphene oxide incorporated collagen-fibrin biofilm as a wound dressing material. RSC Adv 4(107):62717-62727. https://doi.org/10.1039/C4RA10150B
11. Fawal G, Abu-Serie M, Hassan MA, Elnouby MS (2018) Hydroxyethyl cellulose hydrogel for wound dressing: Fabrication, characterization and in vitro evaluation. Int J Biol Macromol 111: 649-659. https://doi.org/10.1016/j.ijbiomac.2018.01.040
12. Ganesan P (2017) Natural and bio polymer curative films for wound dressing medical applications. Wound Med 18:33-40. https://doi.org/10.1016/j.wndm.2017.07.002
13. Ge L, Xu Y, Li X, Yuan L, Tan H, Li D, Mu C (2018) Fabrication of antibacterial collagen-based composite wound dressing. ACS Sustainable Chem. Eng. 6(7):9153-9166. https://doi.org/10.1021/acssuschemeng.8b01482
14. Gonzalez JS, Ludueña LN, Ponce A, Alvarez VA (2014) Poly(vinyl alcohol)/cellulose nanowhiskers nanocomposite hydrogels for potential wound dressings. Mat Sci Eng C-Mater 34:54-61. https://doi.org/10.1016/j.msec.2013.10.006
15. Harkins AL, Duri S, Kloth LC, Tran CD (2014) Chitosan-cellulose composite for wound dressing material. Part 2. Antimicrobial activity, blood absorption ability, and biocompatibility. J Biomed Mater Res Part B Appl Biomater 102(6):1199-1206. https://doi.org/10.1002/jbm.b.33103
16. He M, Chen H, Zhang X, Wang C, Xu C, Xue Y, Wang J, Zhou P, Zhao Q (2018) Construction of novel cellulose/chitosan composite hydrogels and films and their applications. Cellulose 25: 1987-1996. https://doi.org/10.1007/s10570-018-1683-9
17. Huang W, Wang Y, Huang Z, Wang X, Chen L, Zhang Y, Zhang L (2018) On-demand dissolvable self-healing hydrogel based on carboxymethyl chitosan and cellulose nanocrystal for deep partial thickness burn wound healing. ACS Appl Mater Interfaces 10(48): 41076-41088. https://doi.org/10.1021/acsami.8b14526
18. Huang X, Zhang Y, Zhang X, Xu L, Chen X, Wei S (2013) Influence of radiation crosslinked carboxymethyl-chitosan/gelatin hydrogel on cutaneous wound healing. Mat Sci Eng C-Mater 33(8): 4816-4824. https://doi.org/10.1016/j.msec.2013.07.044
19. Huang Y, Huang J, Cai J, Lin W, Lin Q, Wu F, Luo J (2015) Carboxymethyl chitosan/clay nanocomposites and their copper complexes: Fabrication and property. Carbohyd Polym 134:390-

397. https://doi.org/10.1016/j.carbpol.2015.07.089

20. Jayakumar R, Prabaharan M, Sudheesh Kumar P, Nair S, Tamura H (2011) Biomaterials based on chitin and chitosan in wound dressing applications. Biotechnol Adv 29(3):322-337. https://doi.org/10.1016/j.biotechadv.2011.01.005
21. Kim HR, Jang JW, Park JW (2016) Carboxymethyl chitosan-modified magnetic-cored dendrimer as an amphoteric adsorbent. J Hazard Mater 317:608-616. https://doi.org/10.1016/j.jhazmat.2016.06.025
22. Li HY, Wang MC, Williams GR, Wu J, Sun X, Lv Y, Zhu L (2016) Electrospun gelatin nanofibers loaded with vitamins A and E as antibacterial wound dressing materials. RSC Adv 6(55):50267-50277. https://doi.org/10.1039/C6RA05092A
23. Mogoşanu GD, Grumezescu MA (2014) Natural and synthetic polymers for wounds and burns dressing. Int J Pharmaceut 463(2):127-136. https://doi.org/10.1016/j.ijpharm.2013.12.015
24. Naseri N, Mathew A, Girandon L, Fröhlich M, Oksman K (2015) Porous electrospun nanocomposite mats based on chitosan-cellulose nanocrystals for wound dressing: Effect of surface characteristics of nanocrystals. Cellulose 22:521-534. http://dx.doi.org/10.1007/s10570-014-0493-y
25. Pinho E, Soares G (2018) Functionalization of cotton cellulose for improved wound healing. J Mater Chem B 6(13):1887-1889. https://doi.org/10.1039/C8TB00052B
26. Pourshahrestani S, Zeimaran E, Kadri NA, Gargiulo N, Jindal HM, Naveen SV, Sekaran SD, Kamarul T, Towler MR (2017) Potency and cytotoxicity of a novel gallium-containing mesoporous bioactive glass/chitosan composite scaffold as hemostatic agents. ACS Appl Mater Interfaces 9(37):31381-31392. https://doi.org/10.1021/ acsami.7b07769
27. Rowan MP, Cancio LC, Elster EA, Burmeister DM, Rose LF, Natesan S, Chan RK, Christy RJ, Chung KK (2015) Burn wound healing and treatment: Review and advancements. Crit Care 19:243. https://doi.org/10.1186/s13054-015-0961-2
28. Singaravelu S, Ramanathan G, Raja MD, Barge S, Sivagnanam UT (2015) Preparation and characterization of keratin-based biosheet from bovine horn waste as wound dressing material. Mater Lett 152:90-93. https://doi.org/10.1016/j.matlet.2015.03.088
29. Wahid F, Wang H, Zhong C, Chu L (2017) Facile fabrication of moldable antibacterial carboxymethyl chitosan supramolecular hydrogels cross-linked by metal ions complexation. Carbohyd Polym 165:455-461. https://doi.org/10.1016/j.carbpol.2017.02.085
30. Wang Y, Xiao D, Zhong Y, Zhang L, Chen Z, Sui X, Wang B, Feng X, Xu H, Mao Z (2020) Facile fabrication of carboxymethyl chitosan/paraffin coated carboxymethylated cotton fabric with asymmetric wettability for hemostatic wound dressing. Cellulose 27:3443-3453. https://doi.org/10.1007/s10570-020-02969-2
31. Yan S, Yin J, Tang L, Chen X (2011) Novel physically crosslinked hydrogels of carboxymethyl chitosan and cellulose ethers: Structure and controlled drug release behavior. J Appl Polym Sci 119(4):2350-2358. https://doi.org/10.1002/app.32678

32. Ye S, Jiang L, Wu J, Su C, Huang C, Liu X, Shao W (2018) Flexible amoxicillin-grafted bacterial cellulose sponges for wound dressing: In vitro and in vivo evaluation. ACS Appl Mater Interfaces 10(6):5862-5870. https://doi.org/10.1021/acsami.7b16680
33. Zhang W, Xin Y, Yin B, Ye G, Wang J, Shen J, Li L, Yang Q (2019) Synthesis and properties of crosslinked carboxymethyl chitosan and its hemostatic and wound healing effects on liver injury of rats. J Biomater Appl. https://doi.org/10.1177/0885328219852888
34. Zhou H, Cao P, Li J, Zhang F, Ding P (2015) Preparation and release kinetics of carboxymethyl chitosan/cellulose acetate microspheres as drug delivery system. J Appl Polym Sci 132(26):42152. https://doi.org/10.1002/app.42152

Figures

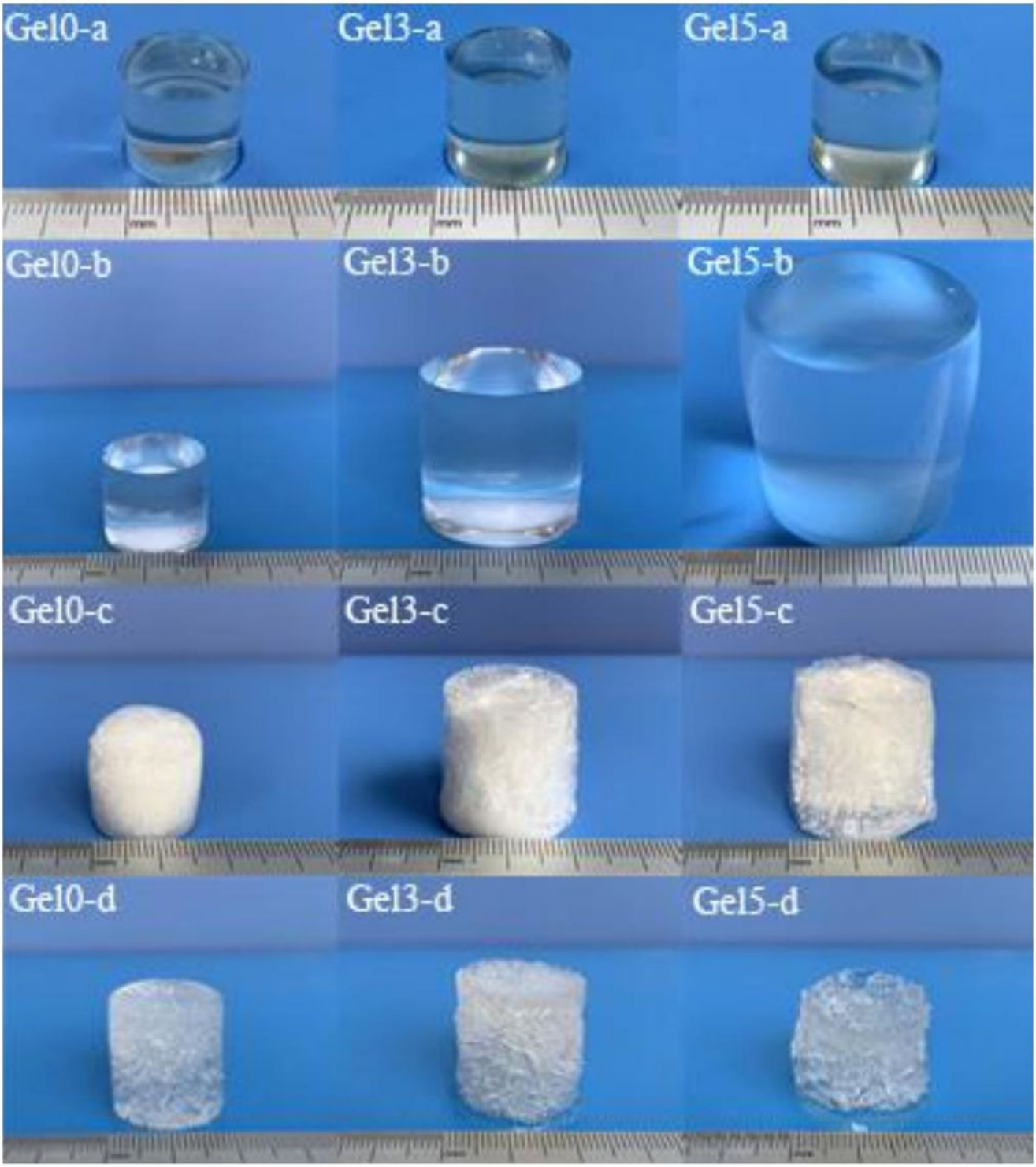

Figure 1

Photographs of the hydrogels at different states: (a) original hydrogels, (b) swollen hydrogels, (c) dried hydrogels and (d) hydrogels after swelling in physical saline water for a week

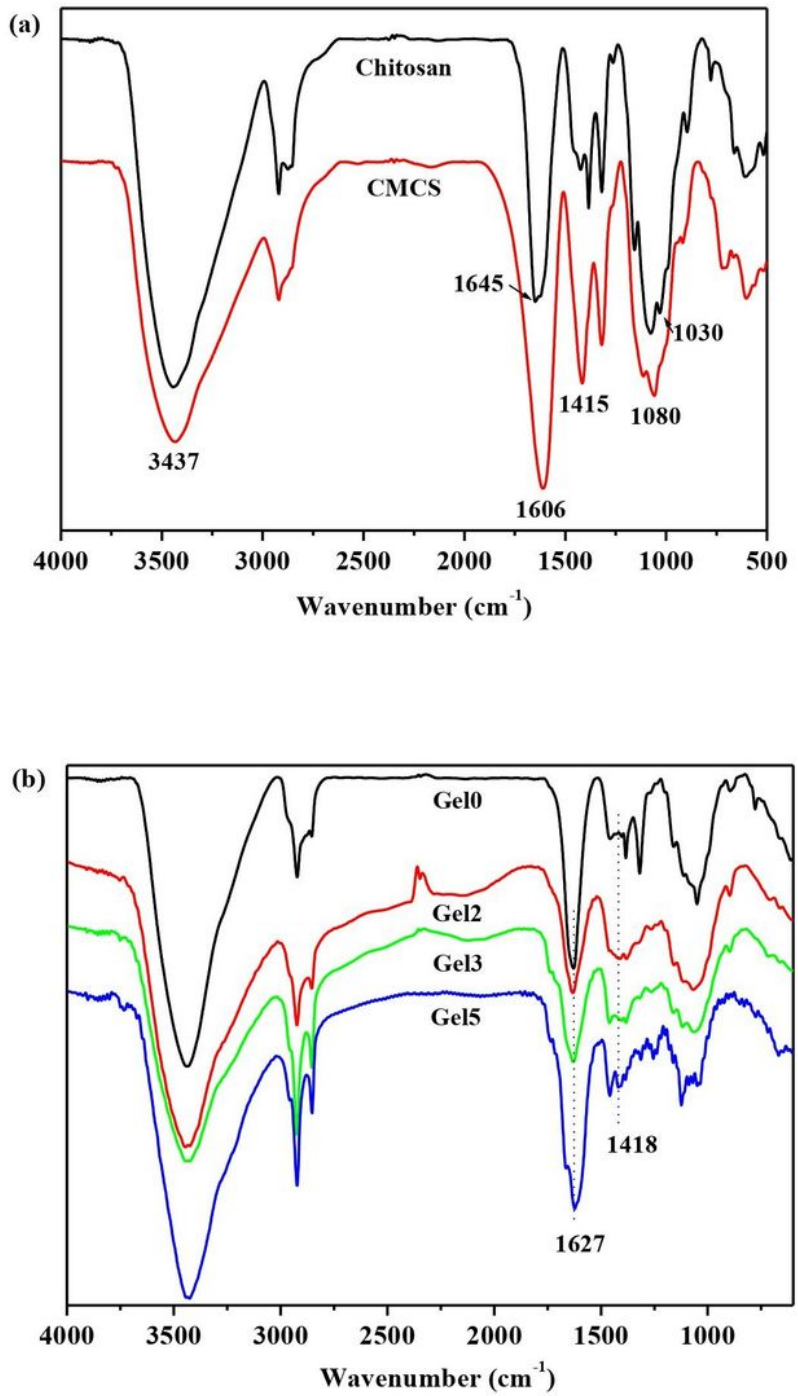

Figure 2

FTIR spectra of (a) chitosan and CMCS, (b) the hydrogels

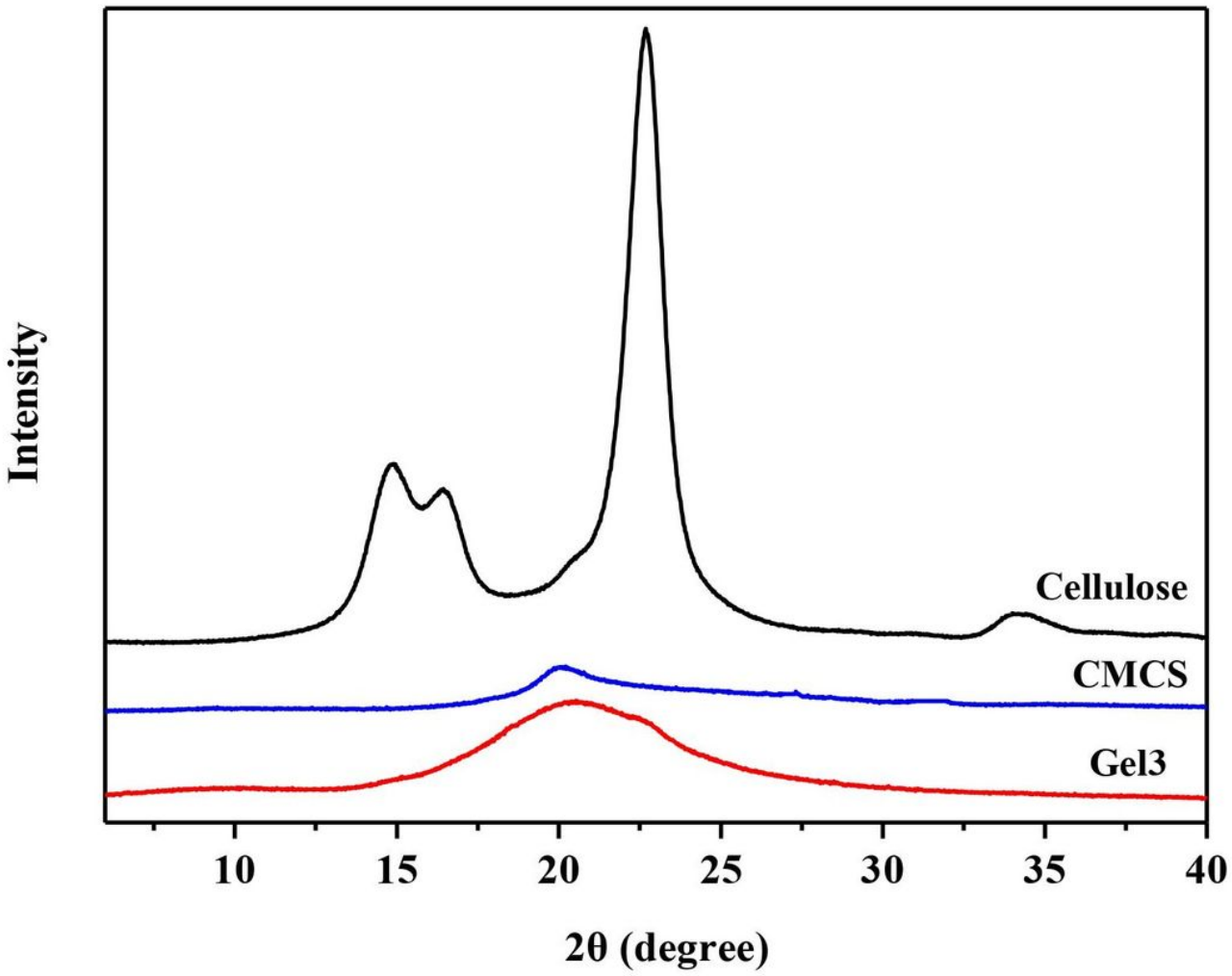

Figure 3

X-ray diffraction patterns of cellulose, CMCS and Gel3

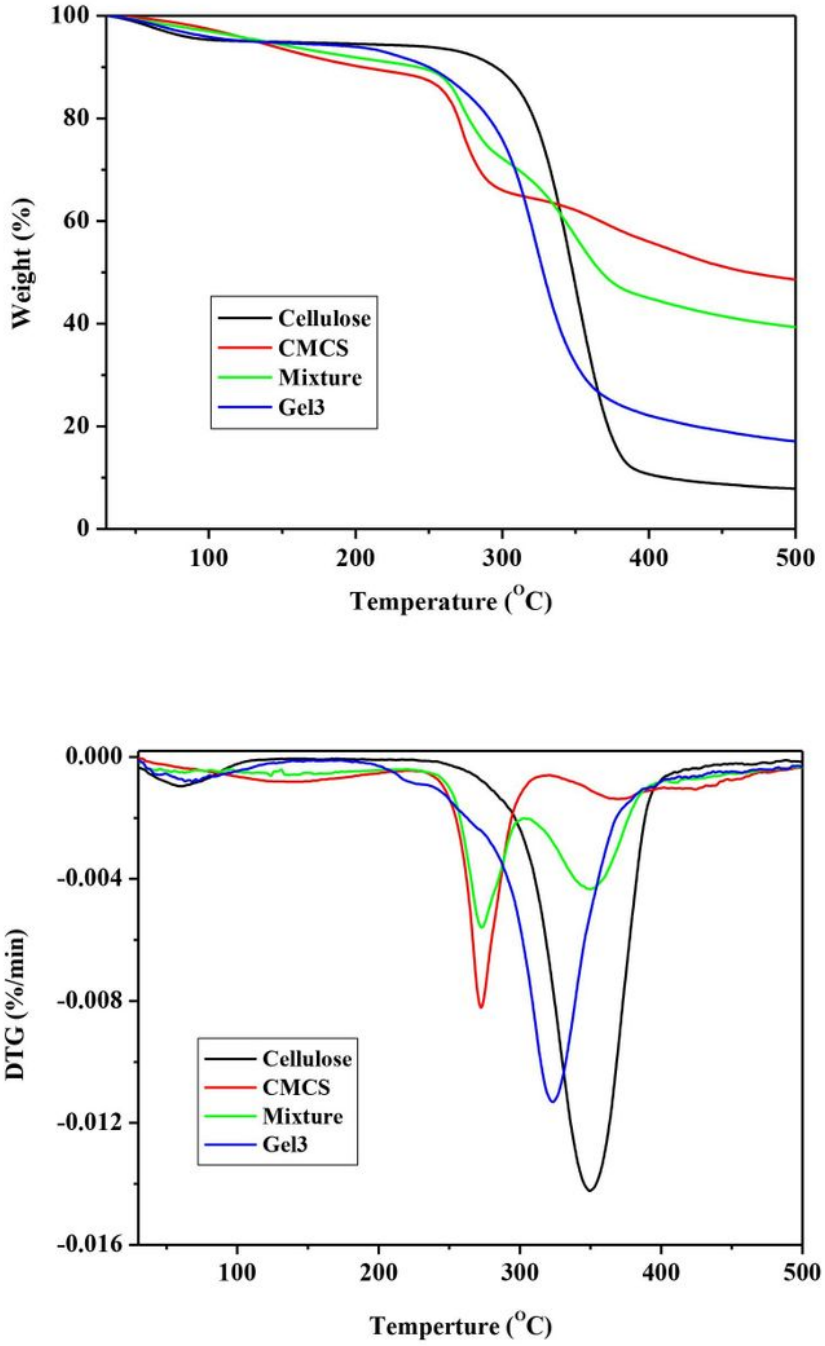

Figure 4

TG and DTG curves of cellulose, CMCS, cellulose/CMCS mixture and Gel3

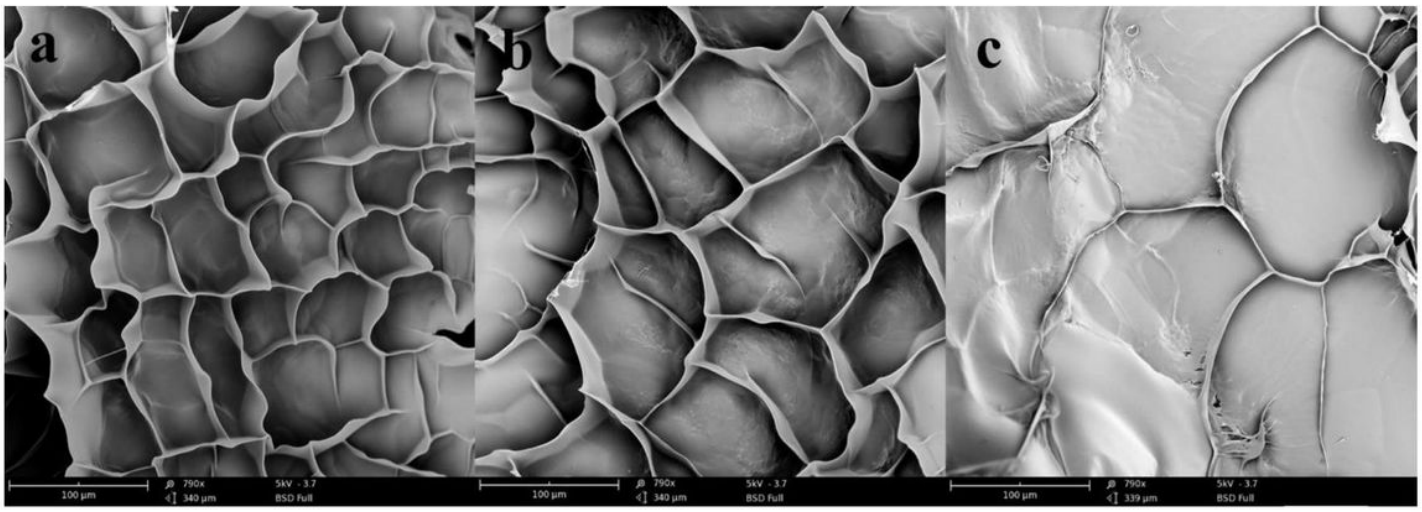

Figure 5

SEM images of the cross-sections of the hydrogels: (a) Gel0, (b) Gel2 and (c) Gel4

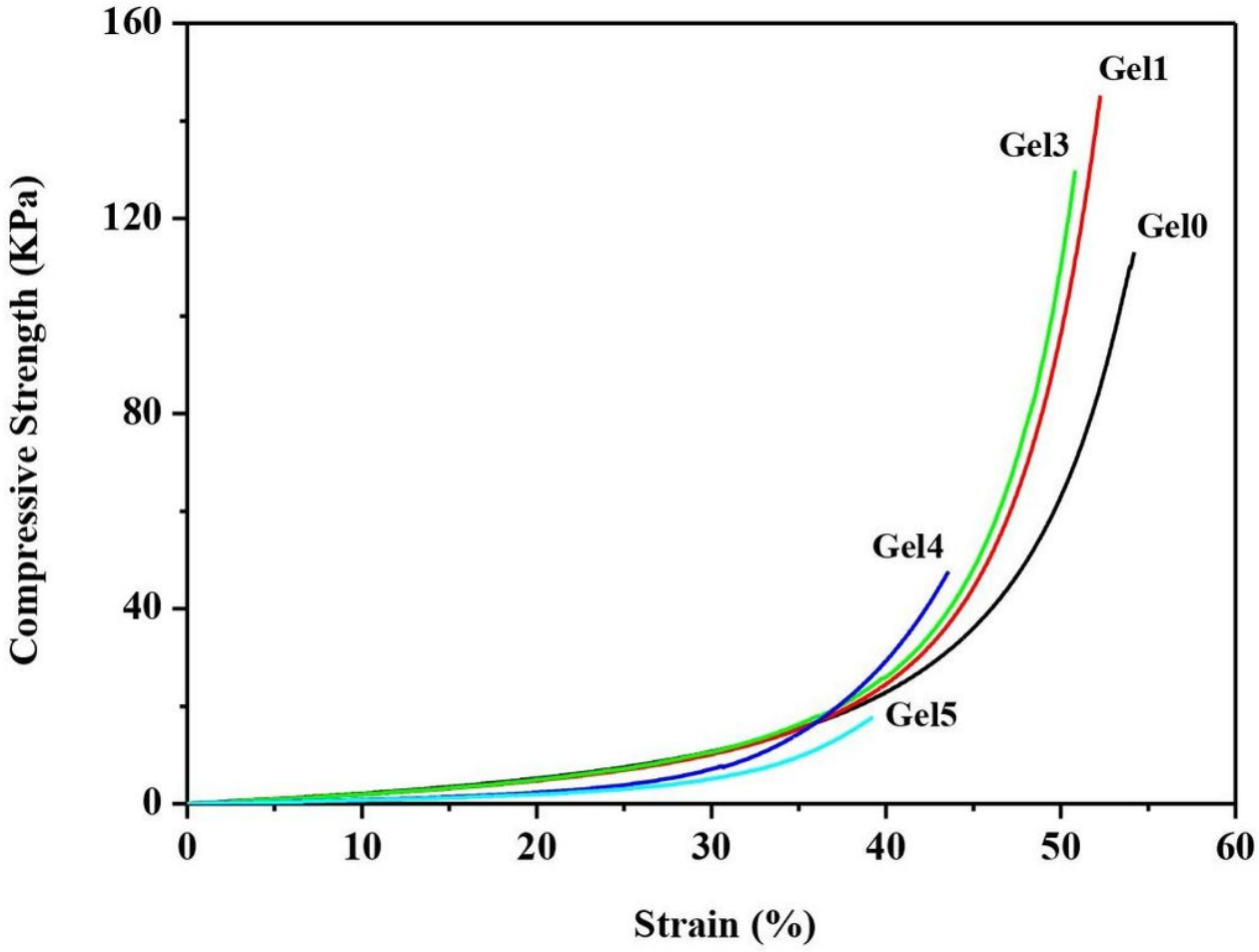

Figure 6

Compressive modulus (σ)-strain (ε) curves of the hydrogels at room temperature

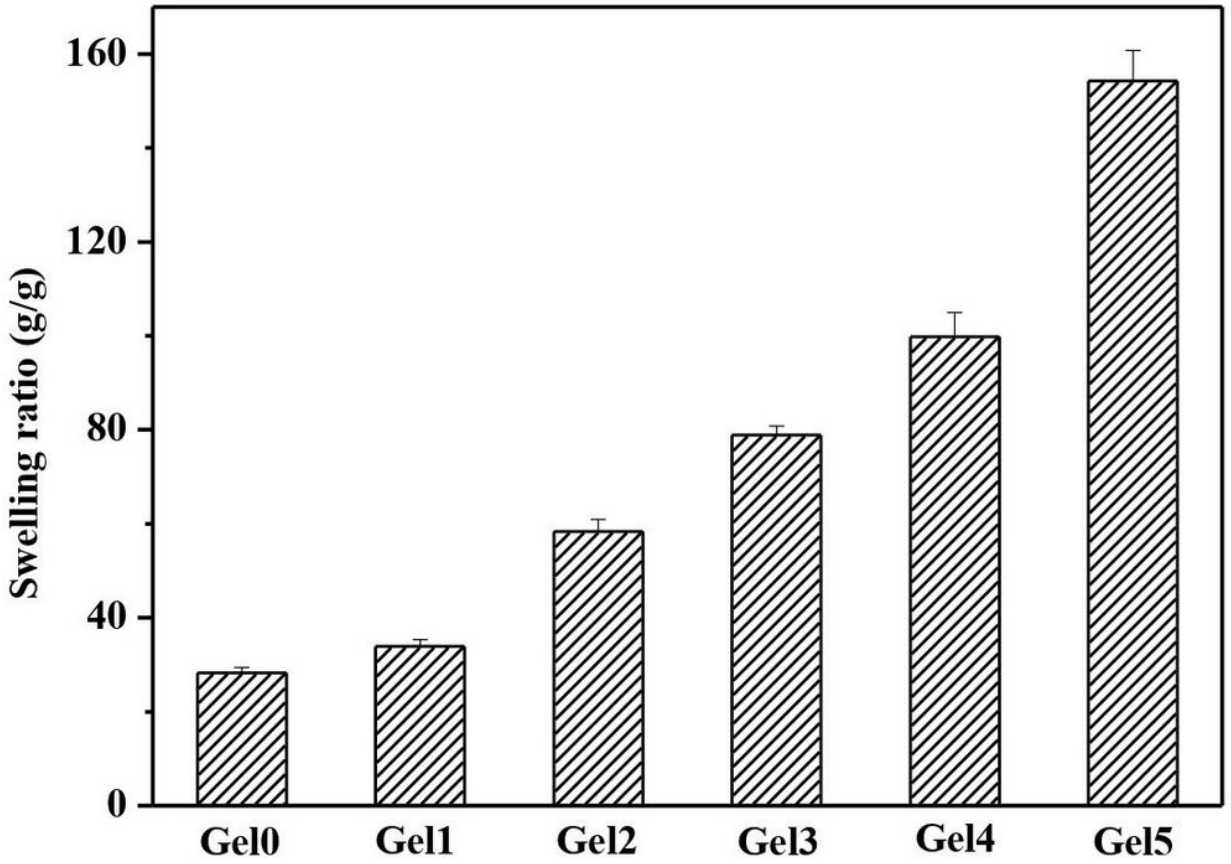

Figure 7

Equilibrium swelling ratios of the hydrogels after immersing in distilled water for a week at 37 ℃

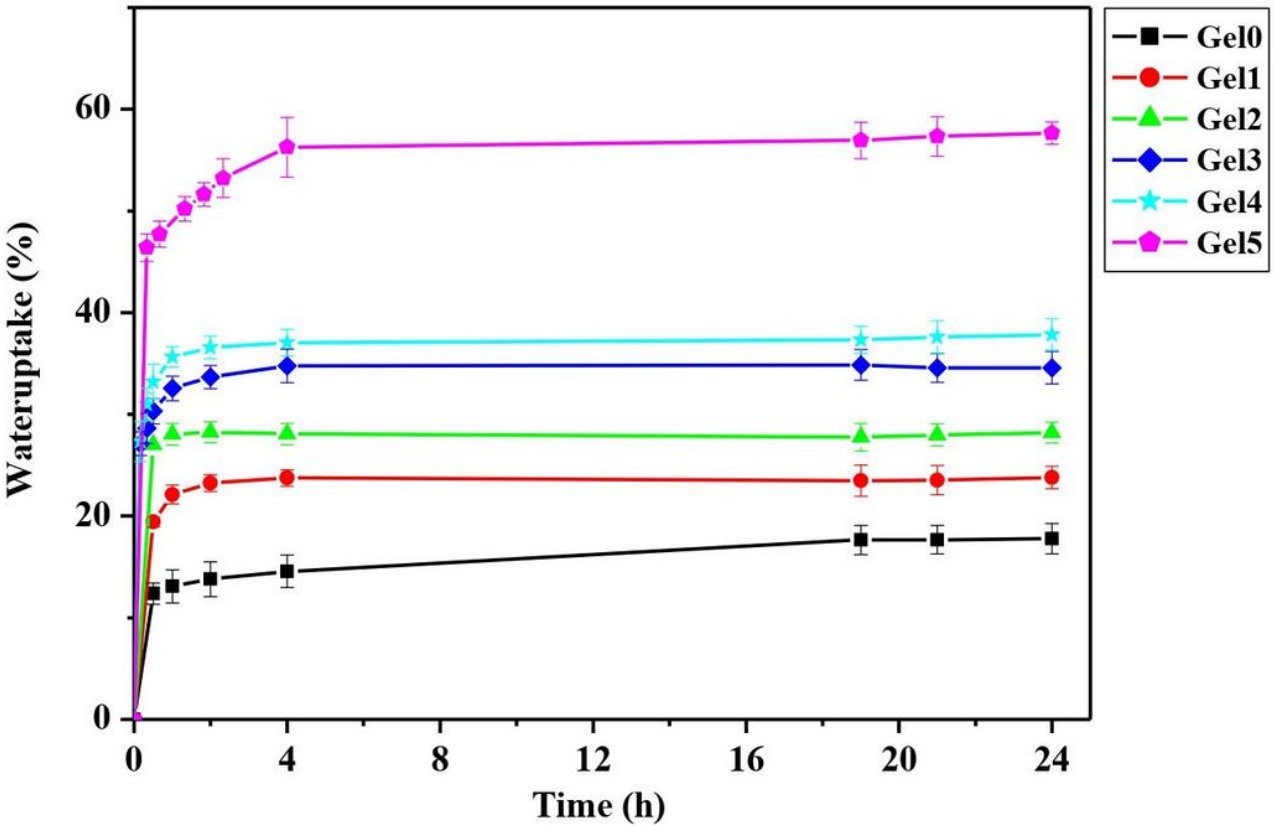

Figure 8

Reswelling kinetic of the hydrogels in distilled water at 37 °C

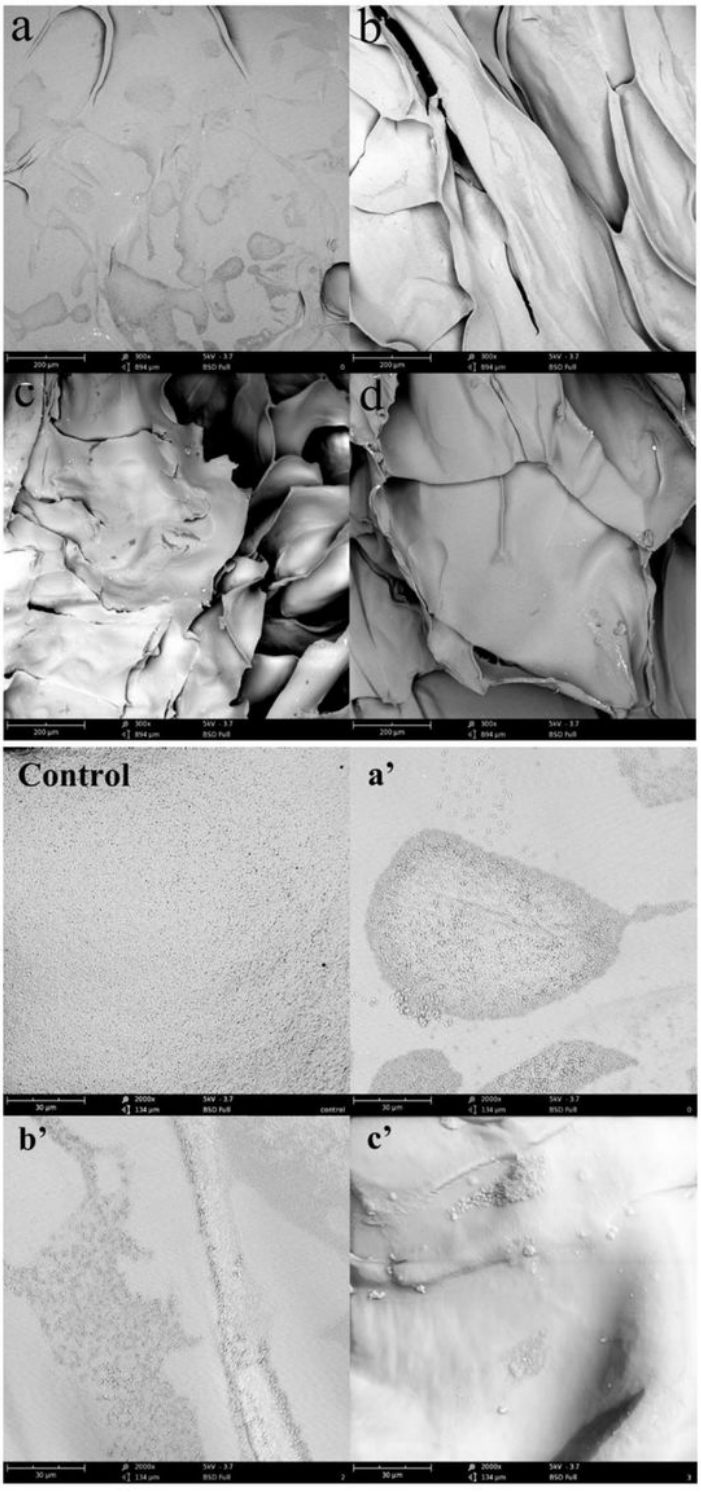

Figure 9

SEM images of the cross-sections of the hydrogels after culturing S. aureus for 24 h: (a) Gel0, (b) Gel2, (c) Gel3, and (d) Gel5 (the scale bar is 200μm); control, (a') Gel0, (b') Gel2 and (c') Gel3 (the scale bar is 30μm)

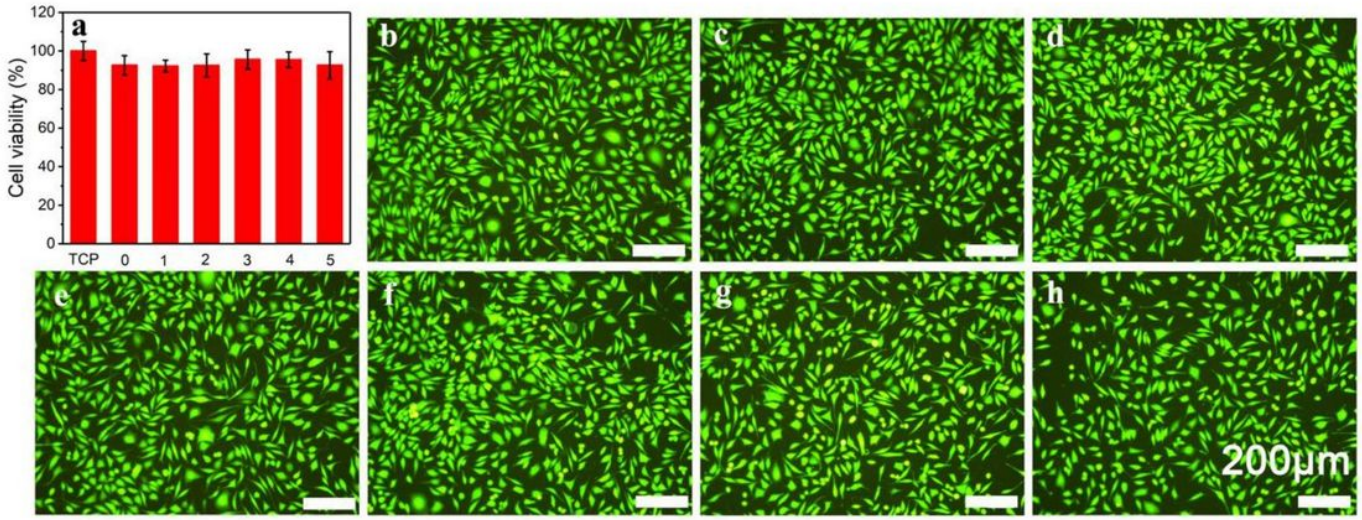

Figure 10

The results of the cytotoxicity tests of hydrogels towards L929 cells after 48 h: (a) cell viability, and images of cells inside hydrogels observed by fluorescent inverted microscope: (b) control, (c) Gel0, (d) Gel1, (e) Gel2, (f) Gel3, (g) Gel4 and (h) Gel5. The scale bar is 200 μm

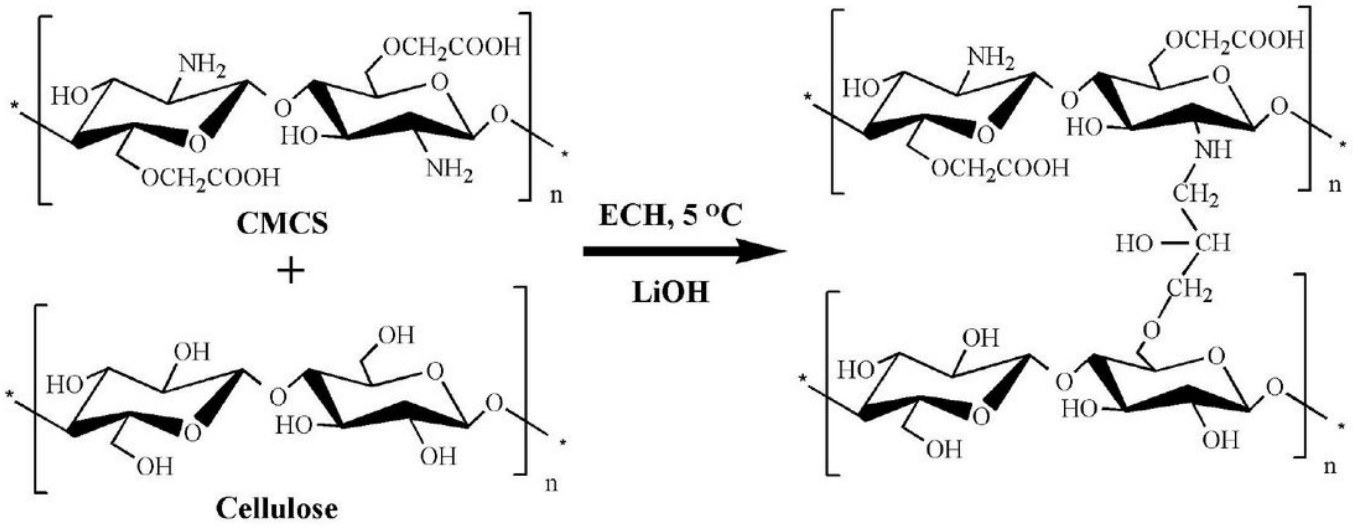

Figure 11

Proposed mechanism for cross-linking reaction of cellulose and CMCS with ECH in LiOH/urea aqueous solution